

Beyond Dense States: Elevating Sparse Transcoders to Active Operators for Latent Reasoning

Yadong Wang^{1,2} Haodong Chen^{1,2} Yu Tian³ Chuanxing Geng^{1,2} Dong Liang^{1,2} Xiang Chen^{1,2}

Abstract

Latent reasoning compresses the chain-of-thought (CoT) into continuous hidden states, yet existing methods rely on dense latent transitions that remain difficult to interpret and control. Meanwhile, sparse representation models uncover human-interpretable semantic features but remain largely confined to post-hoc analysis. We reconcile this tension by proposing **LSTR** (Latent Sparse Transcoder Reasoning), a latent reasoning framework that elevates functional sparse transcoders into active reasoning operators to perform multi-step computation through sparse semantic transitions. At its core, LSTR employs a **Latent Transition Transcoder (LTT)** with a residual skip architecture that decouples linear manifold transport from sparse semantic updates, enabling controllable semantic resolution via explicit sparsity constraints. Extensive experiments show that LSTR preserves reasoning accuracy and compression efficiency while substantially improving interpretability over dense latent baselines. Causal interventions and trajectory analyses further demonstrate that these sparse features act as both interpretable and causally effective operators in the reasoning process.

1. Introduction

Chain-of-Thought (CoT) prompting has significantly enhanced the reasoning performance of large language models (LLMs) by facilitating the explicit decomposition of complex tasks into manageable intermediate steps (Xiang et al., 2025; Wei et al., 2022; Jaech et al., 2024). However, this paradigm introduces a severe computational bottleneck:

¹College of Computer Science and Technology, Nanjing University of Aeronautics and Astronautics, Nanjing, China ²MIIT Key Laboratory of Pattern Analysis and Machine Intelligence, Nanjing, China ³Institute for AI, Tsinghua University, Beijing, China. Correspondence to: Xiang Chen <xiang.chen@nuaa.edu.cn>.

Preprint. February 3, 2026.

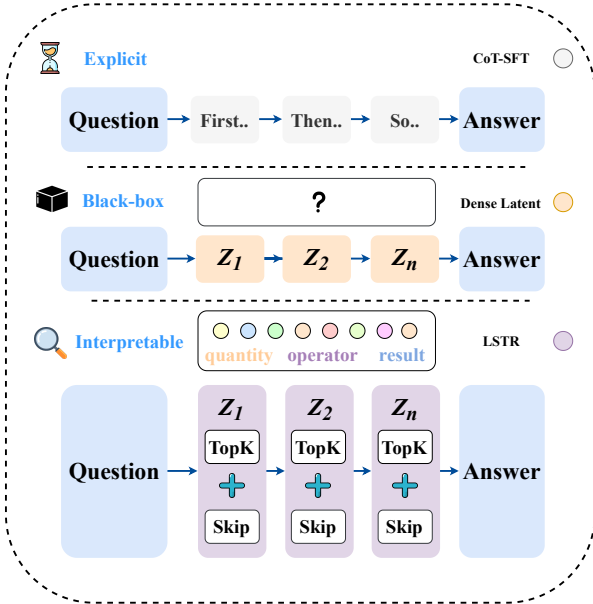


Figure 1. Comparison of reasoning paradigms. CoT relies on long explicit token chains, incurring high latency. Dense latent reasoning compresses computation but lacks interpretability due to fully active latent dimensions. In contrast, LSTR performs reasoning through sparse, interpretable latent features, achieving both efficiency and semantic control.

generating extensive token-level chains inflates inference latency and memory footprints, hindering deployment in time-sensitive or resource-constrained applications. The inherent coupling between reasoning depth and the number of autoregressively decoded tokens creates a linear scaling of costs that becomes prohibitive as task complexity increases.

To mitigate this inefficiency, recent work has explored **latent reasoning**, where intermediate reasoning steps are compressed into continuous hidden representations rather than explicit tokens (Cheng & Durme, 2024; Saunshi et al., 2025; Chen et al., 2025). This dense formulation renders the latent reasoning process an opaque and unstructured substrate, making the underlying reasoning dynamics difficult to interpret, analyze, or control. Methods such as **Coconut** (Hao et al., 2024) and **CoLaR** (Tan et al., 2025) demonstrate that

multiple reasoning steps can be folded into a small number of latent transitions, substantially reducing inference cost. However, existing latent reasoning approaches almost exclusively rely on dense latent representations, in which all latent dimensions are simultaneously active at each step.

In parallel, advances in mechanistic interpretability have shown that dense neural representations can often be decomposed into sparse sets of semantically meaningful features. Sparse autoencoders and transcoder models have been successfully applied to uncover human-interpretable concepts in frozen language models. Nevertheless, these approaches remain largely post-hoc: sparse features are extracted for analysis, but do not participate in or influence the model’s reasoning dynamics during inference.

This separation exposes a fundamental gap between two research directions: latent reasoning compresses computation but sacrifices interpretability, while sparse feature learning provides interpretability but remains detached from reasoning. This gap motivates a central question: *can sparse, interpretable structures be elevated from passive diagnostic to active operators that drive latent reasoning?*

We answer this question affirmatively by introducing **LSTR** (**L**atent **S**parse **T**ranscoder **R**easoning), a framework that reformulates latent reasoning as a sequence of transitions through a sparse semantic feature space. Instead of performing reasoning in dense hidden states, LSTR enforces an explicit sparsity bottleneck at each latent step, ensuring that only a small number of semantic features are activated and updated. At the core of LSTR is the **Latent Transition Transcoder (LTT)**, which combines a linear skip pathway with a sparse nonlinear semantic pathway to decouple background transport from reasoning-specific updates. Sparsity in LSTR is not a post-hoc regularizer, but an architectural principle that governs how reasoning computation is allocated across latent dimensions.

A direct consequence of this formulation is **semantic resolution control**: by adjusting the sparsity budget k , LSTR explicitly regulates the number of active semantic features. This provides a principled mechanism for trading off reasoning granularity against efficiency and enables systematic analysis of how reasoning capacity is distributed. Through extensive experiments and causal interventions, we show that sparse latent reasoning yields stable features corresponding to meaningful roles (e.g., arithmetic operations) while preserving performance. Our contributions are:

- We introduce **LSTR**, the first framework to elevate sparse transcoders from post-hoc analysis tools to active reasoning operators.
- We introduce **semantic resolution control** via explicit sparsity constraints, enabling systematic regulation of latent reasoning capacity.

- Through extensive experiments and causal interventions, we demonstrate that sparse latent reasoning preserves reasoning performance while substantially improving interpretability and controllability.

2. Related Work

2.1. Latent and Implicit Reasoning

Explicit CoT generation incurs substantial overhead and latency (Wei et al., 2022). To address this limitation, **latent reasoning** internalizes reasoning processes into continuous hidden representations (Zhu et al., 2025). While early methods like iCoT (Deng et al., 2024) absorb reasoning supervision into parameters, recent works explicitly model latent trajectories. Coconut (Hao et al., 2024) introduces a “chain of continuous thought” by recursively feeding hidden states back into the model, enabling exploration over latent reasoning paths. CODI (Shen et al., 2025) further aligns student latent states with teacher reasoning hidden states via self-distillation. CoLaR (Tan et al., 2025) subsequently implements dynamic compression and optimizes trajectories using reinforcement learning. Despite their effectiveness in reducing inference cost, these approaches rely almost exclusively on **dense** latent representations, in which all latent dimensions are jointly active at each transition. This dense formulation limits interpretability and controllability, as individual latent dimensions lack clear semantic attribution. In contrast, our work introduces an explicit sparse semantic bottleneck, enabling latent transitions to be composed of localized and interpretable functional features.

2.2. Sparse Transcoders and Feature Learning

Sparse Autoencoders (SAEs) disentangle polysemantic neurons into interpretable semantic features (Bricken et al., 2023). More recently, **Transcoders** extend this paradigm by modeling the functional input–output behavior rather than reconstructing static activations (Dunefsky et al., 2024). Empirical studies show that transcoders capture substantially more interpretable features by directly approximating the operational semantics of neural submodules (Paulo et al., 2025). Architectural refinements such as Skip Transcoders alleviate the rank limitations imposed by sparse bottlenecks through affine residual pathways, while Ghost Gradients revive underutilized features by propagating residual signals to inactive units. Together, these improve dictionary utilization and mechanistic interpretability. However, existing sparse feature learning remains primarily a post-hoc diagnostic tool for static and frozen models. In contrast, our work repurposes sparse transcoders as *active reasoning operators*, training sparse features to directly govern latent state transitions and integrating interpretability into the intrinsic core dynamics of latent reasoning itself.

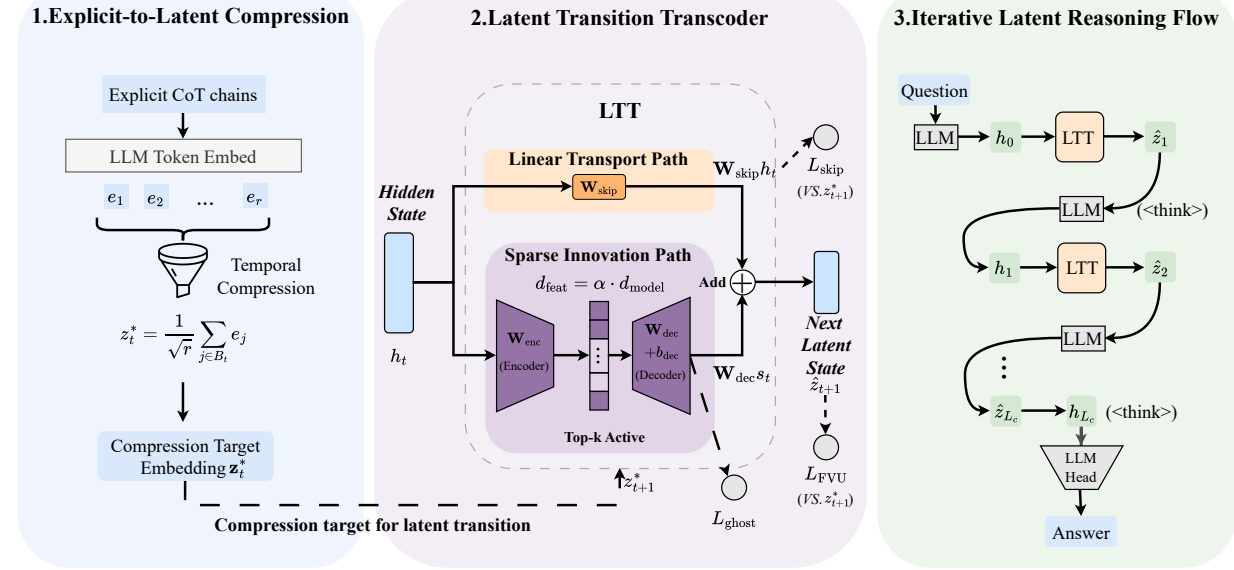


Figure 2. Overview of **LSTR**. A contiguous sequence of explicit reasoning tokens is temporally aggregated into a compressed target embedding. At each latent step, the Latent Transition Transcoder (LTT) performs a bilateral decomposition of the transition dynamics: a linear Transport Path maintains manifold continuity, while a Sparse Innovation Path (via Top- k selection) injects interpretable semantic updates. Under a fixed (r, k) budget, LSTR enables Semantic Resolution Control, where different sparse activation patterns correspond to distinct reasoning primitives such as arithmetic operations or logic gates.

3. Methodology

3.1. Overview of LSTR

We introduce **LSTR** (Latent Sparse Transcoder Reasoning), a framework that reformulates latent reasoning as a compressed trajectory governed by explicit sparsity constraints. At its core lies the **Latent Transition Transcoder (LTT)**, an active operator that transforms dense backbone activations into structured latent transitions.

LSTR strategically decomposes each latent transition into two functionally distinct and complementary components: a linear transport path that preserves manifold continuity, and a sparse innovation path that injects localized semantic updates. This bilateral decomposition alleviates the rank limitations imposed by hard sparsity while ensuring that each latent transition remains both stable and interpretable.

Unlike dense latent reasoning, where all latent dimensions are simultaneously active and entangled, LSTR enforces a structured allocation of reasoning computation. The skip pathway captures predictable background drift in the latent manifold, while the sparse pathway focuses exclusively on reasoning-relevant residual semantics. As a result, sparsity in LSTR is not merely a regularization technique, but an architectural principle that governs how reasoning capacity is distributed across latent dimensions.

As illustrated in Fig. 2, LSTR is trained via supervised tra-

jectory imitation, where compressed latent targets derived from explicit reasoning chains guide the learning of sparse latent transitions. The following sections describe how latent trajectories are constructed, how sparse transitions are parameterized, and how stability and feature utilization are ensured during training.

3.2. Latent Trajectory Mapping and Alignment

LSTR maps explicit reasoning tokens T_r to a compressed latent trajectory $\mathcal{Z}^* = \{z_1^*, \dots, z_{L_c}^*\}$ with a fixed compression ratio r , where $L_c = \lceil L_r/r \rceil$. This compression transforms long reasoning chains into compact latent sequences while preserving their global semantic structure.

Following (Tan et al., 2025), each block of r embeddings B_t is aggregated using **sqrt pooling**:

$$z_t^* = \frac{1}{\sqrt{r}} \sum_{j \in B_t} e_j. \quad (1)$$

This normalization preserves variance scale and prevents latent magnitude inflation with increasing compression ratios. The resulting latent targets are further standardized using the empirical embedding variance to ensure numerical stability during supervision.

Training is performed on the concatenated sequence $[E_q, <\text{think}>, \mathcal{Z}^*, <\text{think}>, E_a]$ under a dual objective. At each latent step t , the LTT predicts the next latent state

$\hat{\mathbf{z}}_{t+1}$ from the hidden state \mathbf{h}_t , supervised by \mathbf{z}_{t+1}^* . Meanwhile, the language modeling head predicts a **randomly sampled token** from the corresponding block \mathcal{B}_{t+1} .

This stochastic token supervision anchors latent dynamics to discrete semantics without full token generation. Random sampling avoids positional bias, fostering broader semantic grounding across the compressed block.

3.3. Latent Transition Transcoder

The **Latent Transition Transcoder (LTT)** predicts the next latent state $\hat{\mathbf{z}}_{t+1}$ from the backbone hidden state \mathbf{h}_t . To overcome the representational bottleneck imposed by hard sparsity, LTT decomposes latent transitions into two functionally specialized paths:

$$\hat{\mathbf{z}}_{t+1} = \mathbf{W}_{\text{skip}} \mathbf{h}_t + \mathbf{W}_{\text{dec}} \mathbf{s}_t + \mathbf{b}_{\text{dec}}, \quad (2)$$

$$\mathbf{s}_t = \text{Top-}k(\sigma(\mathbf{W}_{\text{enc}}(\mathbf{h}_t - \mu) + \mathbf{b}_{\text{enc}})). \quad (3)$$

Here, $\mathbf{W}_{\text{skip}} \in \mathbb{R}^{d \times d}$ is a zero-initialized, bias-free linear adapter modeling smooth manifold transport. The sparse innovation branch projects activations into a high-dimensional dictionary ($d_{\text{feat}} = \alpha d_{\text{model}}$), facilitating the disentanglement of fine-grained reasoning primitives. We define $\sigma(\cdot)$ as the ReLU activation and the Top- k operator as the semantic resolution bottleneck, enforcing hard sparsity by retaining the k largest activations in \mathbf{s}_t . To improve selectivity, we remove global bias using an empirical mean μ and constrain decoder columns to unit norm ($\|\mathbf{W}_{\text{dec}}^{(i)}\|_2 = 1$) to prevent scale collapse. This decouples linear background drift from nonlinear semantic innovations, significantly enhancing training stability and mechanistic interpretability under stringent sparsity constraints.

3.4. Optimization and Feature Utilization

The LTT is optimized via a composite latent objective, where gradients propagate through the Top- k bottleneck using a Straight-Through Estimator (STE):

$$\mathcal{L}_{\text{latent}} = \mathcal{L}_{\text{FVU}} + \lambda_s \mathcal{L}_{\text{skip}} + \lambda_g \mathcal{L}_{\text{ghost}}. \quad (4)$$

Fraction of Variance Unexplained. To account for varying activation magnitudes across reasoning steps, we minimize the **Fraction of Variance Unexplained (FVU)** instead of raw squared error. By normalizing residual energy with target variance, FVU provides a scale-invariant criterion that ensures consistent supervision across different compression ratios and latent depths:

$$\mathcal{L}_{\text{FVU}} = \frac{\mathbb{E}\|\hat{\mathbf{z}}_{t+1} - \mathbf{z}_{t+1}^*\|_2^2}{\text{Var}(\mathbf{z}_{t+1}^*)}. \quad (5)$$

Skip Alignment. This objective prevents semantic innovation from leaking into the linear transport path by forcing the skip branch to approximate the dominant manifold drift:

$$\mathcal{L}_{\text{skip}} = \mathbb{E}\|(\mathbf{W}_{\text{skip}} \mathbf{h}_t + \mathbf{b}_{\text{dec}}) - \mathbf{z}_{t+1}^*\|_2^2. \quad (6)$$

Feature Revitalization. Under hard sparsity ($k \ll d_{\text{feat}}$), poorly initialized units may suffer from dead-feature collapse. To maximize dictionary utilization, we employ a **ghost-gradient** mechanism that propagates reconstruction residuals $\mathbf{r}_t = \mathbf{z}_{t+1}^* - \hat{\mathbf{z}}_{t+1}$ to inactive encoder units:

$$\mathcal{L}_{\text{ghost}} = \mathbb{E}\|\mathbf{W}_{\text{dec}} \cdot \text{enc}(\mathbf{h}_t)_{\text{dead}} - \mathbf{r}_t\|_2^2. \quad (7)$$

4. Experiments

We conduct a series of experiments to systematically investigate how latent reasoning is realized in practice, and whether introducing sparse transcoder structures can serve as an effective and interpretable reasoning operator. Our experimental design is guided by the following Research Questions (**RQs**):

- **RQ1:** Does **LSTR** achieve superior accuracy and efficiency compared to dense latent reasoning baselines across diverse mathematical reasoning benchmarks?
- **RQ2:** How are latent transitions mechanistically implemented through sparse activations within the multi-step reasoning trajectories of **LSTR**?
- **RQ3:** Can latent reasoning capacity be explicitly regulated at inference time via the sparsity budget k , without additional retraining?

4.1. Experimental Setup

Datasets. We primarily train and evaluate our models on **GSM8k-Aug** (Deng et al., 2023), an augmented version of GSM8k containing approximately 385k training samples and 1k test samples. To assess generalization across reasoning distributions, we additionally evaluate on three out-of-domain benchmarks: **GSM-Hard** (Gao et al., 2023), **SVAMP** (Patel et al., 2021), and **MultiArith** (Roy & Roth, 2016). For evaluating scalability to more challenging reasoning regimes, we further report results on the **MATH** dataset (Hendrycks et al., 2021). Following prior work (Hao et al., 2024), we report **Accuracy (Acc.)** as the percentage of correctly solved problems and **Reasoning Length (#L)**, measured as the average number of generated reasoning tokens or latent transitions, as a proxy for inference cost.

Baselines. We compare LSTR against the following representative baselines: (1) **CoT** (Wei et al., 2022), fine-tuned on

Table 1. Performance comparison on four grade-school mathematical reasoning benchmarks. We report averaged accuracy (Acc. %) and average latent reasoning length (#L) over five runs with different random seeds, together with 95% confidence intervals (\pm). CoLaR- c and LSTR- r denote models evaluated with different compression ratios. Gray rows indicate ablation variants of LSTR, where *w/o Sparse* removes the sparse transcoder and *w/o Skip* disables the skip connection. Shorter reasoning length indicates more compact latent reasoning trajectories. Unless otherwise specified, ablation variants share the same training protocol, with architectural components disabled during evaluation to isolate their functional contributions.

Method	GSM8k-Aug		GSM-Hard		SVAMP		MultiArith		Average	
	Acc.	# L	Acc.	# L	Acc.	# L	Acc.	# L	Acc.	# L
CoT	49.4 \pm .72	25.6 \pm .11	11.9 \pm .16	34.2 \pm .11	59.8 \pm .29	12.1 \pm .03	93.2 \pm .49	13.7 \pm .09	53.6	21.4
iCoT	19.8 \pm .23	0.00 \pm .00	3.87 \pm .16	0.00 \pm .00	36.4 \pm .51	0.00 \pm .00	38.2 \pm .66	0.00 \pm .00	24.6	0.00
Coconut	23.1 \pm .28	6.00 \pm .00	5.49 \pm .33	6.00 \pm .00	40.7 \pm .65	6.00 \pm .00	41.1 \pm .24	6.00 \pm .00	27.6	6.00
Distill	13.3 \pm .62	6.00 \pm .00	2.97 \pm .24	6.00 \pm .00	21.7 \pm .73	6.00 \pm .00	19.2 \pm .83	6.00 \pm .00	14.3	6.00
CoLaR-5	26.8 \pm .17	5.57 \pm .02	5.87 \pm .10	6.53 \pm .01	48.4 \pm .45	2.95 \pm .02	86.4 \pm .35	3.21 \pm .01	41.7	4.57
CoLaR-2	40.1 \pm .20	12.7 \pm .02	9.08 \pm .03	14.0 \pm .07	54.9 \pm .20	6.11 \pm .01	91.3 \pm .12	7.35 \pm .01	48.8	10.0
LSTR-5	29.5 \pm .32	5.69 \pm .00	6.29 \pm .12	6.75 \pm .00	49.2 \pm .49	3.03 \pm .00	88.2 \pm .14	3.17 \pm .00	43.3	4.66
- w/o Skip	27.5 \pm .09	5.75 \pm .00	5.52 \pm .16	7.95 \pm .00	50.5 \pm .59	3.18 \pm .00	84.1 \pm .32	3.23 \pm .00	41.9	5.0
- w/o Sparse	20.7 \pm .29	5.80 \pm .00	4.44 \pm .11	6.58 \pm .00	41.7 \pm .48	3.11 \pm .00	75.8 \pm .29	3.38 \pm .00	35.6	4.7
LSTR-2	40.2 \pm .09	13.18 \pm .00	8.81 \pm .06	18.51 \pm .00	53.9 \pm .29	6.47 \pm .00	90.5 \pm .29	7.44 \pm .00	48.4	11.4
- w/o Skip	35.3 \pm .19	13.14 \pm .00	7.9 \pm .12	24.41 \pm .00	53.1 \pm .29	6.69 \pm .00	92.8 \pm .21	7.37 \pm .00	47.3	12.9
- w/o Sparse	34.2 \pm .22	13.43 \pm .00	7.32 \pm .17	23.37 \pm .00	48.6 \pm .36	6.49 \pm .00	85.3 \pm .37	7.57 \pm .00	43.9	12.7

complete reasoning chains, performs token-by-token reasoning before outputting answers; (2) **iCoT** (Deng et al., 2024), gradually internalizes reasoning steps and directly generates answers without intermediate tokens; (3) **Coconut** (Hao et al., 2024), progressively replaces token reasoning with latent steps through curriculum learning, executing fixed-length latent reasoning; (4) **Distill** (Shen et al., 2025), distills token-level CoT into fixed-length latent reasoning steps and infers similarly to Coconut. (5) **CoLaR** (Tan et al., 2025), performs dynamic latent reasoning with compression, trained for speed-adjustable inference.

Implementation Details. All models are implemented based on the Llama-3.2-1B-Instruct backbone (Team, 2024). We freeze the backbone parameters and employ LoRA for parameter-efficient fine-tuning. To ensure a fair comparison, all baselines are implemented using the open-source codebase provided by CoLaR and trained under identical random seeds. Following (Tan et al., 2025), each model is trained for a maximum of 50 epochs or 12 hours, with the checkpoint achieving the highest validation accuracy selected for final evaluation. For LSTR, we set the latent feature expansion factor to 16 and maintain a sparsity budget of $k = 128$ active features per latent step. All experiments are conducted on two NVIDIA RTX PRO6000 GPUs. Additional configuration details are provided in Appendix Section A.

4.2. Main Results

For **RQ1**, we evaluate whether LSTR achieves competitive reasoning performance and efficiency relative to existing

explicit and implicit reasoning baselines. Table 1 summarizes the accuracy and average reasoning length across four mathematical benchmarks.

Comparison with Baseline Methods. Relative to standard Chain-of-Thought (CoT), LSTR attains competitive accuracy while substantially reducing reasoning length. Although CoT achieves the highest accuracy on some benchmarks, it relies on verbose reasoning chains. In contrast, LSTR maintains robust performance with significantly shorter latent trajectories, demonstrating that sparse latent transitions can effectively substitute explicit textual chains with superior inference efficiency.

Regarding various representative implicit reasoning methods (i.e., iCoT, Coconut, Distill, and CoLaR), we observe that while aggressive compression shortens trajectories, it often leads to severe accuracy degradation, particularly on the challenging GSM-Hard benchmark. Compared with these dense latent baselines, LSTR achieves competitive or superior accuracy under equivalent compression ratios. Specifically, at $r = 5$, LSTR outperforms CoLaR-5 on GSM8k-Aug and GSM-Hard while maintaining comparable performance on SVAMP and MultiArith. At $r = 2$, LSTR achieves similar overall accuracy to CoLaR-2 with slightly fewer reasoning steps on average. These results indicate that introducing structured sparsity into latent transitions preserves reasoning capability under compression, leading to more robust latent reasoning dynamics.

Ablation Analysis. We further analyze the contributions of individual architectural components in LSTR. Removing

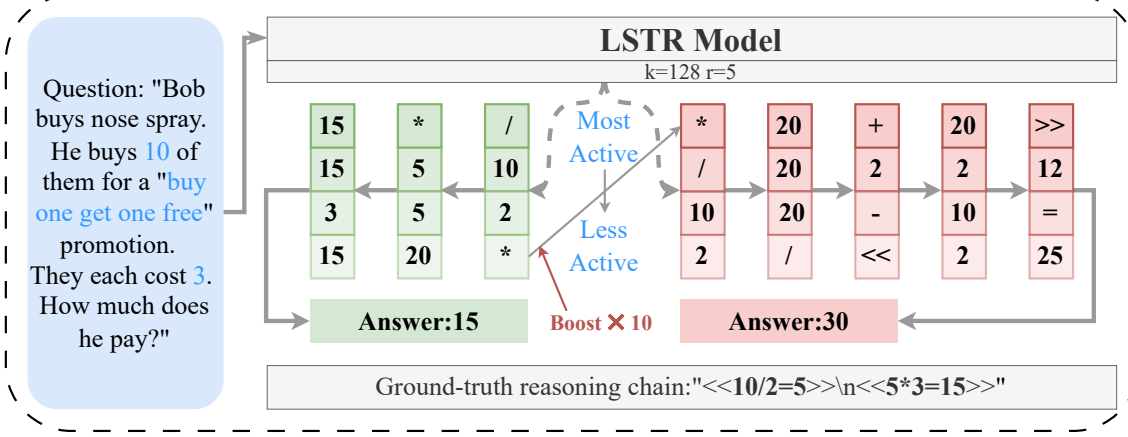


Figure 3. Mechanistic case study of sparse latent reasoning in LSTR. **Left:** Feature activations along a correct trajectory. **Right:** Perturbing a single feature causally diverts the reasoning path and answer correctness.

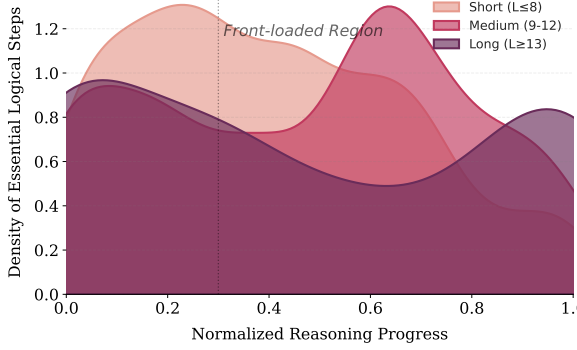


Figure 4. **Causal Necessity Distribution** ($r = 2$). KDE-estimated probability density of essential logical steps across heterogeneous lengths ($L \in [4, 35]$). All balanced cohorts exhibit a consistent front-loaded profile.

the sparse transcoder (refer to *w/o Sparse* in Table 1) consistently degrades accuracy across all datasets; under lower compression ratios (e.g., $r = 2$), it also results in longer and less stable trajectories. Disabling the skip pathway (*w/o Skip*) leads to noticeable accuracy drops, particularly on GSM-Hard and GSM8k-Aug, and similarly increases reasoning length at $r = 2$. These findings indicate that sparse semantic features are essential for effective latent reasoning, while the skip pathway plays a crucial role in stabilizing transitions by absorbing predictable background drift. Together, these ablations confirm that both components are indispensable for achieving an optimal balance between accuracy, efficiency, and stability in sparse latent reasoning.

4.3. Mechanistic Analysis of Sparse Latent Reasoning

For **RQ2**, we investigate the mechanistic implementation of latent reasoning in LSTR at the level of individual sparse

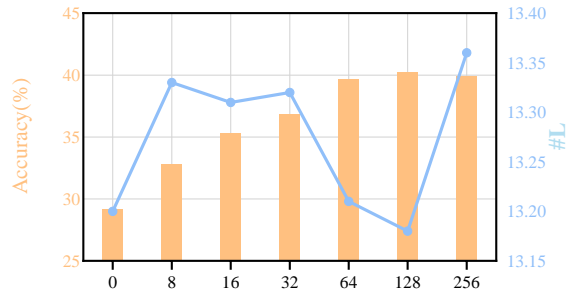


Figure 5. Accuracy and average latent reasoning length under varying inference-time sparsity budgets k . The model is trained with $r = 2$ and $k = 128$, and evaluated by adjusting k at inference time, effectively controlling the capacity of sparse latent transitions.

features and examine whether these features exert a causal influence on the reasoning trajectory. To this end, we combine step-wise latent inspection, targeted feature-level interventions, and large-scale causal sensitivity analysis.

Step-wise Sparse Latent Reasoning Trajectory. We first analyze how sparse latent features evolve during a successful reasoning process. Figure 3 illustrates a representative example from GSM8k-Aug. The model is prompted with an arithmetic word problem and produces a sequence of latent reasoning steps before emitting the final answer. At each latent step, only a sparse subset of features is activated. By decoding the top-activated features via cosine similarity to the token embedding space, we observe a clear semantic progression: early steps predominantly activate quantity- and operator-related features (e.g., 10, /, 2), while later steps increasingly concentrate on result-oriented semantics (e.g., 15). Despite the absence of explicit symbolic supervision during training, this evolution closely mirrors the

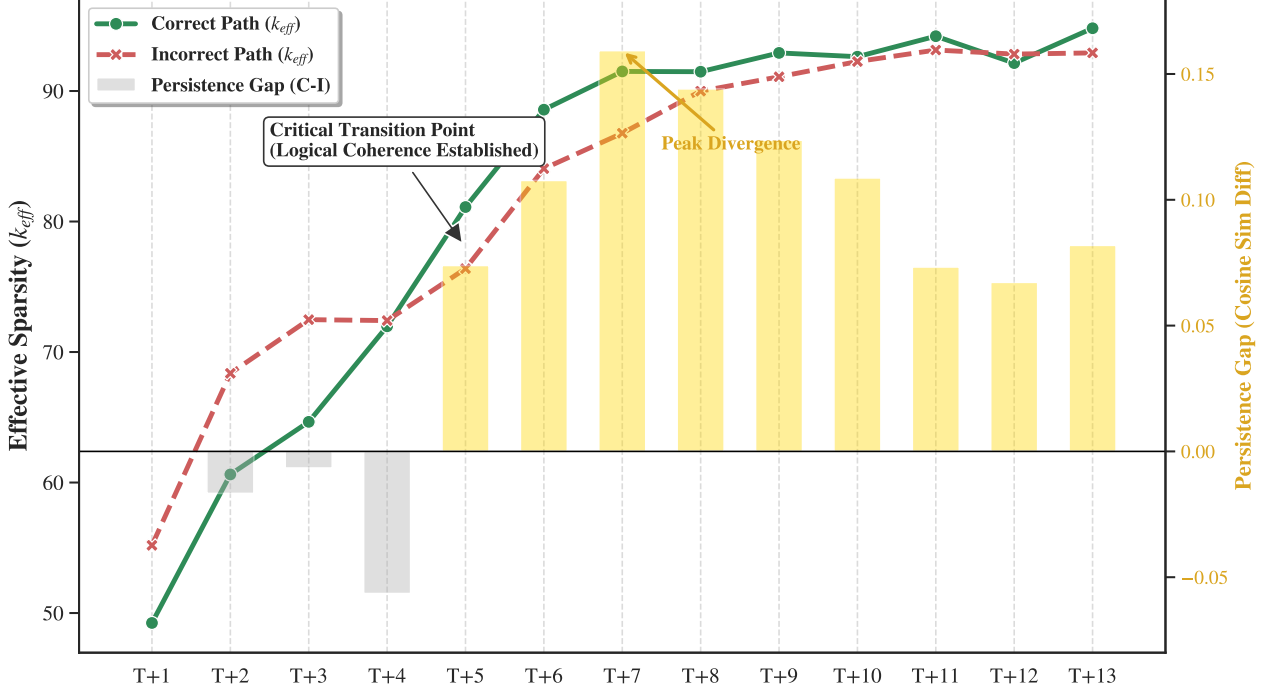


Figure 6. Step-wise effective sparsity k_{eff} and feature persistence along latent reasoning trajectories. The model is trained with $r = 2$ and $k = 128$; sparsity is fixed at inference time. Correct and incorrect trajectories are aggregated separately.

underlying arithmetic logic. Crucially, unlike dense representations, sparse features in LSTR are explicitly indexed and persistent, enabling direct inspection of which semantic components dominate each stage of reasoning.

Causal Feature-Level Intervention. To verify that these sparse features are causally active rather than merely correlational, we perform targeted feature-level interventions. Specifically, we identify a highly active feature in an early step associated with a multiplication operator and manually amplify its activation during inference. As shown in Figure 3, this single-feature intervention substantially and fundamentally alters the downstream latent transitions. Although the model initially activates similar quantity-related features, the subsequent trajectory deviates from the original path and ultimately leads to an incorrect final answer. This demonstrates that individual sparse features in LSTR act as interpretable reasoning operators that exert direct causal control over the underlying computation, rather than serving as passive diagnostic by-products.

Step-wise Causal Sensitivity Analysis. We evaluate reasoning necessity through systematic and large-scale causal ablation on normalized trajectories ($L \in [4, 35]$). As illustrated by the probability density in Figure 4, the *causal necessity*, defined as the density of steps whose ablation triggers reasoning failure, exhibits a consistent “front-loaded” pattern across all cohorts. Regardless of trajectory length,

necessity peaks are concentrated within the initial 30% of progress, confirming that LSTR establishes core semantic commitments early in the reasoning chain. Conversely, the low density in terminal stages ($0.6 \sim 1.0$) suggests a transition toward refinement, where the LTT’s linear transport path maintains manifold stability against sparse perturbations. This causal role is further supported by our qualitative case study (Figure 3), where interventions on early stage features successfully diverted the reasoning outcome, while terminal steps remained robust to such manipulations.

4.4. Explicit Control and Utilization of Reasoning Capacity

For **RQ3**, we design two complementary experiments to examine how reasoning capacity is explicitly regulated via sparsity and utilized during latent reasoning. The first experiment studies inference-time control of the sparsity budget k , evaluating its effect on accuracy and reasoning length. The second experiment goes beyond aggregate metrics and performs a step-wise mechanistic analysis, investigating how sparse latent capacity is allocated and stabilized along successful and failed reasoning trajectories.

Inference-Time Control of Sparsity Budget k . We investigate the impact of inference-time sparsity under a fixed compression ratio $r = 2$. As shown in Figure 5, accuracy increases monotonically and smoothly with larger k , while

Table 2. Scalability to 7B+ backbones on the MATH benchmark. All models utilize $r = 2$ and $k = 128$. LSTR maintains a consistent efficiency-accuracy trade-off across different model families, demonstrating that sparse latent transitions can successfully internalize complex symbolic dependencies in larger parameter spaces.

Method	DeepSeek-R1-Distill-Qwen-7B		Llama-3.2-8B-Instruct	
	Acc.	# L	Acc.	# L
CoT	$35.2 \pm .31$	198.0 ± 1.2	$24.1 \pm .27$	200.0 ± 1.5
CoLaR	$16.5 \pm .14$	$81.2 \pm .23$	$8.0 \pm .19$	$85.4 \pm .44$
LSTR	$15.9 \pm .11$	$72.9 \pm .00$	$10.9 \pm .23$	$82.9 \pm .01$

the average latent reasoning length remains nearly constant. When k is small, the model exhibits performance degradation due to capacity-limited reasoning, whereas performance saturates beyond a moderate sparsity budget. Crucially, k regulates the number of active semantic features at inference time without requiring any expensive model retraining. This demonstrates that LSTR enables zero-shot regulation of reasoning capacity through sparse latent operators.

Latent Capacity Utilization and Trajectory Stability. We further analyze how sparse capacity is deployed by examining step-wise effective sparsity k_{eff} and feature persistence. As illustrated in Figure 6, while correct and incorrect trajectories exhibit similar average sparsity, their internal latent dynamics differ substantially. In early steps, incorrect trajectories activate a larger but less stable set of features. In contrast, correct trajectories gradually concentrate and stabilize their sparse activations. This “late-stage crossover” is accompanied by consistently higher inter-step feature persistence for correct trajectories, indicating significantly more coherent latent transitions. These results suggest that successful reasoning in LSTR is characterized not by raw capacity usage, but by a vastly more structured and temporally consistent deployment of sparse semantic features.

4.5. Scalability to Larger Models

To examine whether sparse latent reasoning generalizes beyond small-scale backbones, we evaluate LSTR on DeepSeek-R1-Distill-Qwen-7B (DeepSeek-AI, 2025) and Llama-3.2-8B-Instruct (Team, 2024). These experiments are conducted on the MATH benchmark, which represents a substantially harder reasoning regime with complex symbolic dependencies. For all scalability evaluations, we maintain a fixed configuration for LSTR with a compression ratio of $r = 2$ and a sparsity budget of $k = 128$, ensuring consistency with the training protocol established in Section 4.1 and providing a fair comparison with the CoLaR baseline under the same compression factor.

Across both DeepSeek and Llama backbones, LSTR consistently produces reasoning trajectories that are considerably more compact than explicit CoT. The framework

maintains its compression advantage at scale, demonstrating that sparse latent transitions can effectively internalize complex reasoning steps even in high-dimensional parameter spaces. While a performance gap relative to CoT persists, likely due to the challenge of capturing intricate symbolic dependencies within a fully latent substrate, the efficiency gains remain remarkably stable. Notably, the performance profile of LSTR is consistent across these distinct model families. Both the accuracy and reasoning length metrics exhibit near-identical patterns for the DeepSeek-based and Llama-based backbones, despite differing architectural origins and distillation backgrounds. This cross-model stability suggests benefits of sparse latent reasoning are intrinsic to the LTT architecture rather than backbone-specific artifacts. Overall, these results confirm LSTR provides a structurally consistent and scalable alternative for efficient reasoning in large language models, preserving its core efficiency-interpretability trade-off as backbone capacity grows.

5. Conclusion and Future Work

In this work, we investigate sparse latent reasoning as a controllable and interpretable alternative to explicit chain-of-thought supervision. We propose **LSTR**, a sparse latent reasoning framework built upon the **Latent Transition Transcoder (LTT)** that enables stable multi-step latent transitions under hard sparsity constraints. By decomposing latent dynamics into manifold transport and sparse semantic innovation, LSTR preserves essential reasoning signals while substantially reducing latent reasoning length. Extensive experiments demonstrate that LSTR achieves competitive accuracy compared with existing latent reasoning methods, while providing significantly improved interpretability and controllability. Through systematic mechanistic analyses, we further show that sparse latent features in LSTR are semantically grounded and exert direct causal influence on reasoning trajectories, highlighting sparsity as a structural prior for future reasoning-centric model design. Future work will focus on improving latent supervision fidelity, scaling sparse latent reasoning to larger and multimodal models, and strengthening the alignment between sparse latent semantics and symbolic reasoning representations.

Impact Statement

This paper presents work whose goal is to advance the field of Machine Learning. There are many potential societal consequences of our work, none which we feel must be specifically highlighted here.

References

Bricken, T., Templeton, A., Batson, J., Chen, B., Jermyn, A., Conerly, T., Turner, N. L., Anil, C., Denison, C., Askell, A., Lasenby, R., Wu, Y., Kravec, S., Schiefer, N., Maxwell, T., Joseph, N., Tamkin, A., Nguyen, K., McLean, B., Burke, J. E., Hume, T., Carter, S., Henighan, T., and Olah, C. Towards monosemanticity: Decomposing language models with dictionary learning. <https://transformer-circuits.pub/2023/monosemantic-features/index.html>, 2023.

Chen, Y., Shang, J., Zhang, Z., Xie, Y., Sheng, J., Liu, T., Wang, S., Sun, Y., Wu, H., and Wang, H. Inner thinking transformer: Leveraging dynamic depth scaling to foster adaptive internal thinking. In Che, W., Nabende, J., Shutova, E., and Pilehvar, M. T. (eds.), *Proceedings of the 63rd Annual Meeting of the Association for Computational Linguistics (Volume 1: Long Papers)*, ACL 2025, Vienna, Austria, July 27 - August 1, 2025, pp. 28241–28259. Association for Computational Linguistics, 2025. URL <https://aclanthology.org/2025.acl-long.1369/>.

Cheng, J. and Durme, B. V. Compressed chain of thought: Efficient reasoning through dense representations. *CoRR*, abs/2412.13171, 2024. doi: 10.48550/ARXIV.2412.13171. URL <https://doi.org/10.48550/arXiv.2412.13171>.

DeepSeek-AI. Deepseek-r1: Incentivizing reasoning capability in llms via reinforcement learning. *CoRR*, abs/2501.12948, 2025. doi: 10.48550/ARXIV.2501.12948. URL <https://doi.org/10.48550/arXiv.2501.12948>.

Deng, Y., Prasad, K., Fernandez, R., Smolensky, P., Chaudhary, V., and Shieber, S. M. Implicit chain of thought reasoning via knowledge distillation. *CoRR*, abs/2311.01460, 2023. doi: 10.48550/ARXIV.2311.01460. URL <https://doi.org/10.48550/arXiv.2311.01460>.

Deng, Y., Choi, Y., and Shieber, S. M. From explicit cot to implicit cot: Learning to internalize cot step by step. *CoRR*, abs/2405.14838, 2024. doi: 10.48550/ARXIV.2405.14838. URL <https://doi.org/10.48550/arXiv.2405.14838>.

Dunefsky, J., Chlenski, P., and Nanda, N. Transcoders find interpretable LLM feature circuits. In Globersons, A., Mackey, L., Belgrave, D., Fan, A., Paquet, U., Tomczak, J. M., and Zhang, C. (eds.), *Advances in Neural Information Processing Systems 38: Annual Conference on Neural Information Processing Systems 2024, NeurIPS 2024, Vancouver, BC, Canada, December 10 - 15, 2024*, 2024. URL http://papers.nips.cc/paper_files/paper/2024/hash/2b8f4db0464cc5b6e9d5e6bea4b9f308-Abstract-Conference.html.

Gao, L., Madaan, A., Zhou, S., Alon, U., Liu, P., Yang, Y., Callan, J., and Neubig, G. PAL: program-aided language models. In Krause, A., Brunsell, E., Cho, K., Engelhardt, B., Sabato, S., and Scarlett, J. (eds.), *International Conference on Machine Learning, ICML 2023, 23-29 July 2023, Honolulu, Hawaii, USA*, volume 202 of *Proceedings of Machine Learning Research*, pp. 10764–10799. PMLR, 2023. URL <https://proceedings.mlr.press/v202/gao23f.html>.

Hao, S., Sukhbaatar, S., Su, D., Li, X., Hu, Z., Weston, J., and Tian, Y. Training large language models to reason in a continuous latent space. *CoRR*, abs/2412.06769, 2024. doi: 10.48550/ARXIV.2412.06769. URL <https://doi.org/10.48550/arXiv.2412.06769>.

Hendrycks, D., Burns, C., Kadavath, S., Arora, A., Basart, S., Tang, E., Song, D., and Steinhardt, J. Measuring mathematical problem solving with the MATH dataset. In Vanschoren, J. and Yeung, S. (eds.), *Proceedings of the Neural Information Processing Systems Track on Datasets and Benchmarks 1, NeurIPS Datasets and Benchmarks 2021, December 2021, virtual*, 2021. URL <https://datasets-benchmarks-proceedings.neurips.cc/paper/2021/hash/be83ab3ecd0db773eb2dc1b0a17836a1-Abstract-round2.html>.

Jaech, A., Kalai, A., Lerer, A., Richardson, A., El-Kishky, A., Low, A., Helyar, A., Madry, A., Beutel, A., Carney, A., Iftimie, A., Karpenko, A., Passos, A. T., Neitz, A., Prokofiev, A., Wei, A., Tam, A., Bennett, A., Kumar, A., Saraiva, A., Vallone, A., Duberstein, A., Kondrich, A., Mishchenko, A., Applebaum, A., Jiang, A., Nair, A., Zoph, B., Ghorbani, B., Rossen, B., Sokolowsky, B., Barak, B., McGrew, B., Minaiev, B., Hao, B., Baker, B., Houghton, B., McKinzie, B., Eastman, B., Lugaressi, C., Bassin, C., Hudson, C., Li, C. M., de Bourcy, C., Voss, C., Shen, C., Zhang, C., Koch, C., Orsinger, C., Hesse, C., Fischer, C., Chan, C., Roberts, D., Kappler, D., Levy, D., Selsam, D., Dohan, D., Farhi, D., Mely, D., Robinson, D., Tsipras, D., Li, D., Oprica, D., Freeman, E., Zhang, E., Wong, E., Proehl, E., Cheung, E., Mitchell, E., Wallace, E., Ritter, E., Mays, E., Wang, F., Such, F. P., Raso, F., Leoni, F., Tsimpourlas, F., Song, F., von Lohmann, F., Sulit, F., Salmon, G., Parascandolo, G., Chabot, G.,

Zhao, G., Brockman, G., Leclerc, G., Salman, H., Bao, H., Sheng, H., Andrin, H., Bagherinezhad, H., Ren, H., Lightman, H., Chung, H. W., Kivlichan, I., O’Connell, I., Osband, I., Gilaberte, I. C., and Akkaya, I. Openai o1 system card. *CoRR*, abs/2412.16720, 2024. doi: 10.48550/ARXIV.2412.16720. URL <https://doi.org/10.48550/arXiv.2412.16720>.

Patel, A., Bhattacharya, S., and Goyal, N. Are NLP models really able to solve simple math word problems? In Toutanova, K., Rumshisky, A., Zettlemoyer, L., Hakkani-Tür, D., Beltagy, I., Bethard, S., Cotterell, R., Chakraborty, T., and Zhou, Y. (eds.), *Proceedings of the 2021 Conference of the North American Chapter of the Association for Computational Linguistics: Human Language Technologies, NAACL-HLT 2021, Online, June 6-11, 2021*, pp. 2080–2094. Association for Computational Linguistics, 2021. doi: 10.18653/V1/2021.NAA CL-MAIN.168. URL <https://doi.org/10.18653/v1/2021.naacl-main.168>.

Paulo, G., Shabalin, S., and Belrose, N. Transcoders beat sparse autoencoders for interpretability. *CoRR*, abs/2501.18823, 2025. doi: 10.48550/ARXIV.2501.18823. URL <https://doi.org/10.48550/arXiv.2501.18823>.

Roy, S. and Roth, D. Solving general arithmetic word problems. *CoRR*, abs/1608.01413, 2016. URL <http://arxiv.org/abs/1608.01413>.

Saunshi, N., Dikkala, N., Li, Z., Kumar, S., and Reddi, S. J. Reasoning with latent thoughts: On the power of looped transformers. In *The Thirteenth International Conference on Learning Representations, ICLR 2025, Singapore, April 24-28, 2025*. OpenReview.net, 2025. URL <https://openreview.net/forum?id=din01GfZFd>.

Shen, Z., Yan, H., Zhang, L., Hu, Z., Du, Y., and He, Y. CODI: compressing chain-of-thought into continuous space via self-distillation. *CoRR*, abs/2502.21074, 2025. doi: 10.48550/ARXIV.2502.21074. URL <https://doi.org/10.48550/arXiv.2502.21074>.

Tan, W., Li, J., Ju, J., Luo, Z., Luan, J., and Song, R. Think silently, think fast: Dynamic latent compression of LLM reasoning chains. *CoRR*, abs/2505.16552, 2025. doi: 10.48550/ARXIV.2505.16552. URL <https://doi.org/10.48550/arXiv.2505.16552>.

Team, L. The llama 3 herd of models. *CoRR*, abs/2407.21783, 2024. doi: 10.48550/ARXIV.2407.21783. URL <https://doi.org/10.48550/arXiv.2407.21783>.

Wei, J., Wang, X., Schuurmans, D., Bosma, M., Ichter, B., Xia, F., Chi, E. H., Le, Q. V., and Zhou, D. Chain-of-thought prompting elicits reasoning in large language models. In Koyejo, S., Mohamed, S., Agarwal, A., Belgrave, D., Cho, K., and Oh, A. (eds.), *Advances in Neural Information Processing Systems 35: Annual Conference on Neural Information Processing Systems 2022, NeurIPS 2022, New Orleans, LA, USA, November 28 - December 9, 2022*, 2022. URL http://papers.nips.cc/paper_files/paper/2022/hash/9d5609613524ecf4f15af0f7b31abca4-Abstract-Conference.html.

Xiang, V., Snell, C., Gandhi, K., Albalak, A., Singh, A., Blagden, C., Phung, D., Rafailov, R., Lile, N., Mahan, D., Castricato, L., Fränken, J., Haber, N., and Finn, C. Towards system 2 reasoning in llms: Learning how to think with meta chain-of-thought. *CoRR*, abs/2501.04682, 2025. doi: 10.48550/ARXIV.2501.04682. URL <https://doi.org/10.48550/arXiv.2501.04682>.

Zhu, R., Peng, T., Cheng, T., Qu, X., Huang, J., Zhu, D., Wang, H., Xue, K., Zhang, X., Shan, Y., Cai, T., Kergan, T., Kembay, A., Smith, A., Lin, C., Nguyen, B., Pan, Y., Chou, Y., Cai, Z., Wu, Z., Zhao, Y., Liu, T., Yang, J., Zhou, W., Zheng, C., Li, C., Zhou, Y., Li, Z., Zhang, Z., Liu, J., Zhang, G., Huang, W., and Eshraghian, J. A survey on latent reasoning. *CoRR*, abs/2507.06203, 2025. doi: 10.48550/ARXIV.2507.06203. URL <https://doi.org/10.48550/arXiv.2507.06203>.

A. More Implementation Details

Model Hyperparameters All experiments are conducted using the `Llama-3.2-1B-Instruct` backbone (Team, 2024). The backbone parameters are frozen throughout training, with all trainable parameters introduced via LoRA adapters. We set the LoRA rank to $r_{\text{LoRA}} = 128$ and the scaling factor to $\alpha_{\text{LoRA}} = 32$ for all experiments. The latent reasoning module adopts a sparse autoencoder architecture, where the latent feature dimension is set to $d_{\text{feat}} = 16 \times d_{\text{model}}$. Unless otherwise specified, the sparsity budget is fixed to $k = 128$ active features per latent step. The SAE encoder is initialized with orthogonal weights, while decoder columns are constrained to unit norm to stabilize feature scaling. The decoder bias is initialized using the empirical mean hidden state computed over the training corpus. The skip-path linear adapter is initialized to zero, ensuring that semantic innovation is initially routed through the sparse path. All latent activations use ReLU nonlinearity, and the latent temperature is fixed to 1.0.

Training and Optimization Protocol All models are trained exclusively using **Supervised Fine-Tuning (SFT)**; we do not employ reinforcement learning or policy optimization in any experiment. We utilize the AdamW optimizer with a base learning rate of 1×10^{-4} and weight decay of 1×10^{-2} . To accommodate the different convergence properties of the backbone and the sparse transcoder, we implement a hierarchical learning rate strategy:

Parameter Group	Learning Rate	Weight Decay	Functional Role
Backbone (LoRA)	1×10^{-4}	0.1	Semantic Adaptation
Skip Shield (\mathbf{W}_{skip})	2×10^{-4}	0.0	Manifold Continuity
SAE Encoder	2×10^{-4}	0.0	Feature Discovery
SAE Decoder	2×10^{-4}	0.0	Structural Reconstruction

The sparsity budget is fixed at $k = 128$ throughout training. Gradient clipping with a maximum norm of 1.0 is applied to stabilize training. All experiments are conducted on **two NVIDIA RTX PRO6000 GPUs** using mixed-precision training. Unless otherwise stated, results are averaged over five random seeds (0–4).

B. Sensitivity Analysis of Compression Ratio r

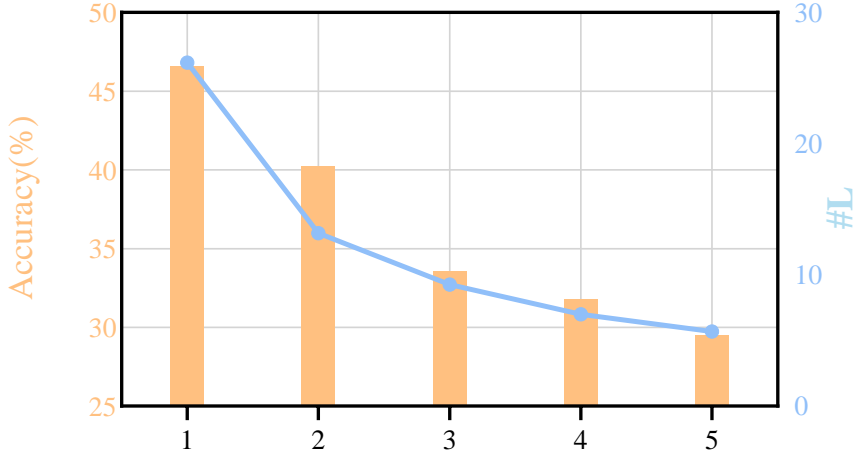


Figure 7. Accuracy and reasoning length (#L) across varying compression ratios r . The orange bars denote reasoning accuracy (%), while the blue line represents the average number of latent reasoning steps (#L) per problem. Increasing r leads to significantly more compact trajectories but results in a corresponding decline in accuracy.

In the main paper, we fix the sparsity budget to $k = 128$ and focus on comparing established latent compression ratios. In this appendix, we provide supplementary results analyzing how the compression strength r affects reasoning performance and trajectory compactness. Specifically, we evaluate LSTR models across a range of compression ratios $r \in \{1, 2, 3, 4, 5\}$, while maintaining a fixed sparsity budget of $k = 128$ and keeping all other hyperparameters constant. Figure 7 illustrates

the corresponding accuracy and average latent reasoning length. As the compression ratio r increases from 1 to 5, the latent trajectory becomes progressively shorter, resulting in substantially and monotonically reduced reasoning length. However, aggressive compression also leads to a gradual degradation in accuracy, reflecting a reduced capacity of the latent manifold to preserve fine-grained reasoning signals under high-pressure bottling. These results demonstrate a clear and smooth accuracy–efficiency Pareto frontier controlled by the compression ratio r , confirming that LSTR enables controllable latent reasoning compression without requiring architectural changes or additional model retraining.

C. Training and Inference Overhead Analysis

We analyze the computational overhead of LSTR relative to explicit CoT and the dense *CoLaR* baseline. All measurements were conducted on a single NVIDIA RTX PRO6000 GPU using FP16 precision with a batch size of 1.

Table 3. Efficiency profiling on GSM8k-Aug. Per-step latency and Peak VRAM were measured during inference. End-to-end (E2E) time is calculated as Average Steps \times Step Latency.

Method	Acc. (%)	Avg. Steps (#L)	Step Latency	Policy Overhead	Peak VRAM
CoT (Explicit)	49.4	25.60	9.26 ms	—	5.14 GB
CoLaR-2 (Dense)	40.1	12.70	8.98 ms	1.69%	5.21 GB
LSTR-2 (Ours)	40.2	13.18	10.66 ms	10.53%	5.66 GB

Inference Latency. As shown in Table 3, LSTR introduces additional computation at each latent step due to the $16\times$ feature expansion in the SAE encoder and the Top- k selection process. Specifically, the **1.02 ms** required for the SAE policy results in a per-step latency of **10.66 ms**, representing a **1.68 ms** increase over the dense baseline (8.98 ms). However, this per-step increase is effectively offset by the reduction in total reasoning length. Compared to explicit CoT, LSTR-2 reduces the reasoning sequence from **25.6** tokens to **13.18** steps. Consequently, the total end-to-end (E2E) inference time for a representative reasoning chain is reduced from **237.1 ms** (CoT) to **140.5 ms** (LSTR-2), achieving a **40.7%** speed improvement. This indicates that LSTR improves efficiency primarily by significantly reducing reasoning length rather than minimizing per-step computation.

Memory and Training. During training, the LLM backbone remains frozen, and overhead arises primarily from sparse feature selection and latent trajectory supervision. The introduction of **138.45 M** parameters in the SAE module increases the peak VRAM usage by approximately **450 MB** compared to the dense model (5.66 GB vs. 5.21 GB) and **520 MB** compared to the CoT baseline. While the static memory footprint is higher, the significantly shorter latent trajectories lead to a slower growth of the **KV Cache** during generation. This makes sparse latent reasoning a practical and scalable alternative to explicit CoT, as the benefits of trajectory compression outweigh the marginal increases in per-step latency and static parameter storage.

D. Latent Structural Analysis

SAE Feature Utilization We analyze the utilization frequency of SAE features by counting their activations under Top- k inference. As shown in Figure 8, the resulting rank–frequency distribution follows a clear power-law pattern. In the full LSTR architecture, feature utilization is highly concentrated, with a Gini coefficient of approximately 0.93, indicating strong specialization of a small subset of latent features. When removing the skip pathway and retaining only the sparse latent path, feature utilization becomes significantly more balanced, with the Gini coefficient reduced to approximately 0.71. This comparison highlights the functional role of the skip pathway in absorbing background structure, allowing sparse features to specialize in discrete semantic innovations.

Latent Semantic Trajectories We further analyze the semantic evolution of latent embeddings across successive reasoning steps. Figure 9 shows the cosine similarity matrix between reconstructed latent embeddings within a single reasoning trajectory. Adjacent latent steps exhibit high similarity, while the similarity between the initial and final steps is substantially lower (Start–End similarity: 0.339), indicating a smooth yet progressive semantic drift. This pattern supports the interpretation that latent reasoning in LSTR follows a coherent semantic trajectory rather than collapsing to static representations or exhibiting random fluctuations.

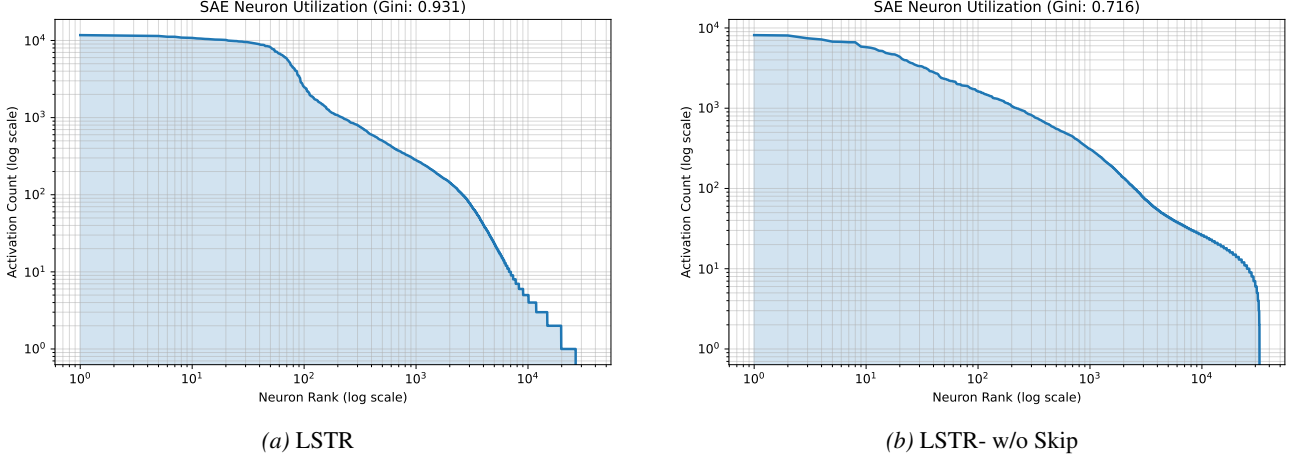


Figure 8. SAE Neuron Utilization Analysis. The rank-frequency distributions follow a clear power-law pattern. (a) In the full LSTR model, the inclusion of the Skip pathway leads to high feature specialization (Gini: 0.931). (b) Without the Skip pathway, the SAE is forced to encode dense background signals, resulting in a more dispersed activation pattern (Gini: 0.716).

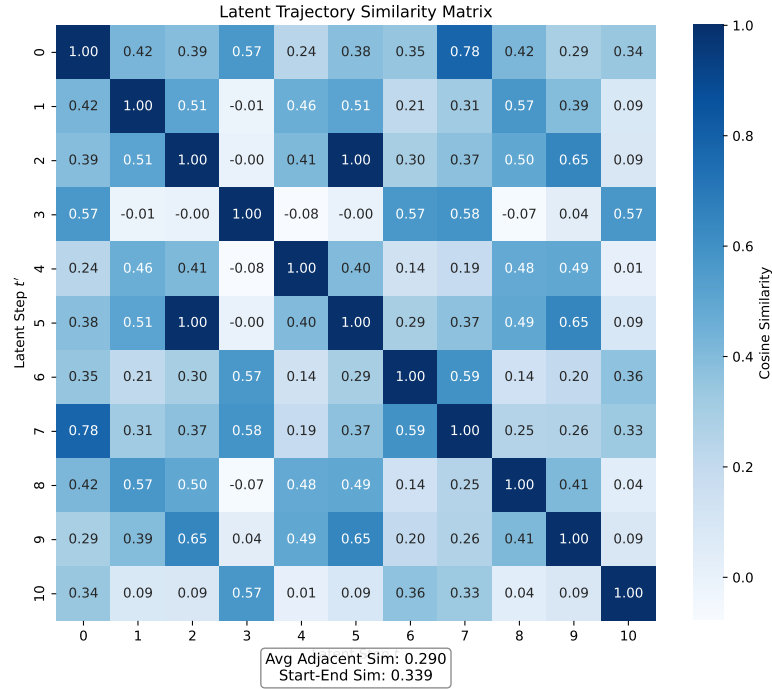


Figure 9. Latent Semantic Trajectory. The cosine similarity matrix of reconstructed latent embeddings $\{h_t\}$ across reasoning steps. The high similarity along the diagonal demonstrates temporal coherence, while the semantic drift from step 1 to the end (Start-End Sim: 0.339) indicates a progressive logical evolution.